1-1-2007

Transport and structural studies of the thermoelectric material, bismuth telluride

Matthew K Jacobsen
University of Nevada, Las Vegas

TRANSPORT AND STRUCTURAL STUDIES OF THE THERMOELECTRIC MATERIAL, BI_2TE_3

by

Matthew K. Jacobsen

Bachelor of Science
Oregon State University
2004

A thesis submitted in partial fulfillment
of the requirements for the

Master of Science Degree in Physics
Department of Physics
College of Sciences

Graduate College
University of Nevada, Las Vegas
May 2007

UNLV
UNIVERSITY OF NEVADA LAS VEGAS

Thesis Approval

The Graduate College
University of Nevada, Las Vegas

April 10th, 20 07

The Thesis prepared by

Matthew Kenneth Jacobsen

Entitled

Transport and Structural Studies of

the Thermoelectric Material, Bi_2Te_3

is approved in partial fulfillment of the requirements for the degree of

Masters of Science in Physics

Examination Committee Chair

Dean of the Graduate College

Examination Committee Member

Examination Committee Member

Graduate College Faculty Representative

1017-53

ABSTRACT

Transport and Structural Studies of the Thermoelectric Material, Bi_2Te_3

by

Matthew K. Jacobsen

Dr. Andrew Cornelius, Examination Committee Chair
Associate Professor of Physics
University of Nevada, Las Vegas

Thermoelectric materials have long been investigated for the possible use as a power source. This application was recently put to use in the Voyager space program to power the deep space probes on their journey. However, the research done in this area has yet to completely study the properties of these special materials. As a result, this research aims to investigate the high pressure structure and transport properties of these materials in a effort to better understand why they behave as they do. To this end, various techniques have been performed revealing the high pressure properties of these matierals.

TABLE OF CONTENTS

ABSTRACT iii

LIST OF FIGURES v

ACKNOWLEDGMENTS vi

CHAPTER 1 INTRODUCTION 1
Properties of Thermoelectrics 2

CHAPTER 2 EXPERIMENTAL BACKGROUND 7
Experimental Techniques 7
Basic Measurements 12
X-Ray Diffraction 12
Electrical Resistivity 13
Thermal Conductivity and Seebeck Coefficient 15
Heat Capacity 19

CHAPTER 3 RESULTS AND DISCUSSION 21
Structure Results 21
Electrical Resistivity 26
Thermal Conductiviy and Seebeck Coefficient 27
Heat Capacity 29
Electronic Topological Transition? 33

CHAPTER 4 CONCLUSIONS 34
Further Work 36

REFERENCES 37

VITA 41

LIST OF FIGURES

Figure 1 Thermogalvanomagnetic Interations [34] 2
Figure 2 Theoretical Heat Capacity Curve [21] 5
Figure 3 Tungsten Carbide Bridgman Cell 8
Figure 4 Merrill Bassett Diamond Anvil Cell 9
Figure 5 Bismuth Resistive Standard Measurement 10
Figure 6 Tungsten Carbide Pressure Calibration Data 10
Figure 7 16 BM-D: EDXRD 13
Figure 8 16 ID-B: ADXRD 13
Figure 9 Diagram of Resistivity Measurements [34] 14
Figure 10 Diagram of Thermal Conductivity Measurements [34] 15
Figure 11 Thermal Conductivity and Seebeck Coefficient Setup 16
Figure 12 Thermal Conductivity Measurement Method Regions 17
Figure 13 PPMS Heat Capacity Puck 20
Figure 14 Crystal Structure of Bi_2Te_3 22
Figure 15 Compression Patterns 23
Figure 16 Decompression Patterns 23
Figure 17 Bi_2Te_3 Compression P vs. V 24
Figure 18 Bi_2Te_3 Decompression P vs. V for four experiments 25
Figure 19 Bi_2Te_3 Resistivity vs. Pressure 26
Figure 20 Bi_2Te_3 Seebeck Coefficient vs. Pressure 27
Figure 21 Bi_2Te_3 Thermal Conductivity vs. Pressure 29
Figure 22 Bi_2Te_3 Heat Capacity 30
Figure 23 Einstein Correction 31
Figure 24 Electronic Correction 32
Figure 25 Gorbachuk Heat Capacity vs. Our Data 32
Figure 26 ZT vs. Pressure for Bi_2Te_3 35

ACKNOWLEDGMENTS

I would like to acknowledge the assistance and support of the following in this project:

Dr. Andrew Cornelius, for putting up with my repeated questions and for advice on many things,

Dr. Ravhi Kumar, for his assistance in learning how to use the required software and techniques,

Dr. Lon Spight, Dr. Michael Pravica, and Dr. Allen Johnson, my stellar graduate committee,

Amadeo Sanchez, James Norton, and Bill O'Donnell, for their wonderful technical toys,

Stanislav Sinogeiken, Yue Meng, H.P. Liermann, for their assistance in the x-ray experiments and experimental design,

Daniel Antonio, Charles Jensen, Jeremy Keen, and Eric Baxter, for their assistance in the experimental process.

Acknowledged Funding and Support Agencies:

Work at UNLV is supported by DOE Cooperative Agreement DE-FC52-06NA27684.

Use of the Advanced Photon Source was supported by the U. S. Department of Energy, Office of Science, Office of Basic Energy Sciences, under Contract No. DE-AC02-06CH11357.

HPCAT is a collaboration among the UNLV High Pressure Science and Engineering Center, Lawrence Livermore National Laboratory, and the Geophysical Laboratory of the Carnegie Institution of Washington.

Additional support for this project was provided by the UNLV Graduate and Professional Student Association.

CHAPTER 1

INTRODUCTION

Solid state physics is rife with various effects caused by the unusual properties of materials. With properties ranging from the generation of light to special properties when exposed to a magnetic field, it would not seem too unlikely that there are materials that are capable of generating electricity under the right conditions. The difference is that these particular materials use heat flow to generate electricity. This complex phenomenon is termed the Seebeck effect. Alternately, the Peltier effect is the reverse of this, using electricity to generate heat flow.

Despite their seeming usefulness, thermoelectric materials have suffered due to poor timing in their discovery, coupled with many other flashy discoveries that occurred during their development. Discovered in 1823 by Seebeck, the property referred to as the Seebeck effect describes the ability of a material to convert heat flow to electricity. This property was discovered when a closed loop made of two different metals was used. Seebeck found that if you heated one of the junctions, the loop would cause a deflection in a compass needle. Although he initially thought that this was due to the earth's magnetic field, he had initiated the field of thermoelectric materials.

Despite this, thermoelectricity would be lost for a time due to the excitement over work on electrodynamics. With the increase of interest in thermodynamics research in the late 1830's, thermoelectric materials would again be pulled into the limelight and, with the help of Peltier and Lenz, Seebeck's work would begin to evolve. However, history has been cruel to thermoelectrics, as they would continue to rise and fall in popularity throughout history. Regardless of the change in interest, there was still a decent amount of progress made in the understanding of this unusual phenomenon.

Some of the greatest contributions to this field occurred in the late 1800's and early 1900's. In 1885, Rayleigh was the first to consider the potential of these materials for

electrical generation. In 1909, Altenkirch provided the first acceptable theories regarding thermoelectricity. In addition, he contributed the fundamental measure of the applicability of a given material, which will be discussed later. The culmination of all of these ideas occurred in 1947, with the advent of the first thermoelectric generator. This device was shown to have a practical operating efficiency of around 5 percent.

Properties of Thermoelectrics

The Seebeck effect is a specific application of the general thermogalvanomagnetic interactions shown in figure 1[1]. In this figure, the Seebeck effect is the same as the Nernst effect with no magnetic field present. By causing a temperature gradient across a thermoelectric, heat flows from one surface to another. In doing so, this causes the material to generate an electrical current. With this idea in mind, the Seebeck coefficient is defined as the ratio of the generated electric field to the temperature gradient across the sample,

$$\alpha = \frac{E_x}{\frac{dT}{dx}} \tag{1.1}$$

where E_x is the transverse electric field and $\frac{dT}{dx}$ is the longitudinal temperature gradient.

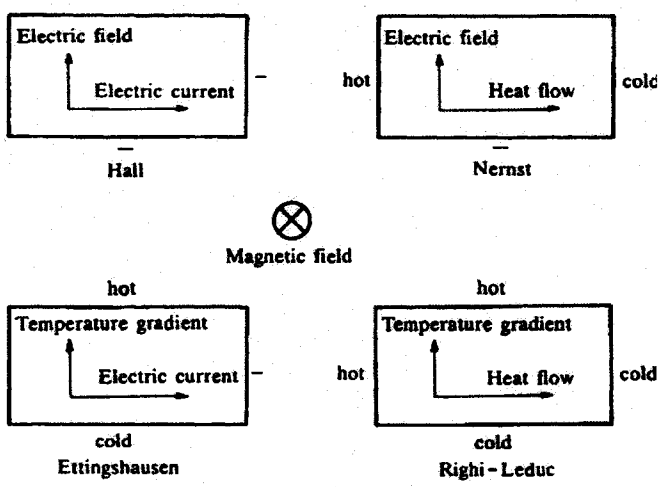

Figure 1 Thermogalvanomagnetic Interations [34]

[1]figure reproduced with permission of Publisher, Springer Verlag

Since the Seebeck effect depends strongly upon current and heat flow through the sample, it is useful to define their relation parameters as well. They are

$$\rho = \frac{E_x}{i_x} \tag{1.2}$$

$$\lambda = \frac{-w_x}{\frac{dT}{dx}} \tag{1.3}$$

where i_x is the current flowing and w_x is the rate of heat flow per unit area. These two equations define the electrical resistivity ρ and the thermal conductivity λ. Earlier, it was mentioned that Altenkirch derived the most useful parameter in describing thermoelectric materials. This parameter is called the figure of merit, Z, and is defined in terms of the previous three parameters as

$$Z = \frac{\alpha^2}{\rho\lambda} \tag{1.4}$$

where Z has units of K^{-1}. Although this parameter is useful, it is rather inconvenient in practice. Since the goal is to find materials useful at room temperature, a more practical parameter is the dimensionless figure of merit ZT, with Z multiplied by the temperature at which it was measured. This ZT parameter is directly related to the thermoelectric engine efficiency. A full derivation of the Z parameter is given in [34]. The ZT parameter typically ranges between 0 and 1.5, depending on the material, with values reported as large as 2 to 3.

The purpose of any thermoelectrics research is to learn enough about the materials and what causes their properties to aid in the search for more desireable materials. This can be remarkably difficult for many reasons. It is necessary to improve the individual parameters of ZT to maximize the performance of the material itself. Looking at each individual parameter, it is obvious that, short of doping the material, there is very little that can be done to improve the Seebeck coefficient α.

As such, it now makes sense to shift attention to the electrical and thermal parameters. Beginning with the thermal conductivity, an understanding is needed about how heat is conducted through the lattice. Fortunately, this theory has existed for quite some time. The theory of crystalline thermal transport, as presented in Kittel [21], is shown to be based on

two sources, the lattice and the charged carriers. The overall thermal conductivity is a sum of these two components

$$\lambda = \lambda_L + \lambda_e \tag{1.5}$$

with λ_L from the lattice and λ_e from the carriers.

The latter of these is highly dependent upon temperature and the concentration of carriers present. The explaination comes from electronic band theory. Using the concept of a free electron Fermi gas, it is easy to show, as done in [21], that electrons at absolute zero occupy all energy levels up to the Fermi level. As soon as the temperature is raised above absolute zero, some of the electrons become thermally excited and begin to move throughout the material as carriers. Since each electron can carry a finite amount of energy from the thermal excitation, the magnitude of the heat transported through the lattice by this method depends on the temperature and the number of electons able to freely move in the lattice. Despite this, the thermal excitation energy at room temperature remains small, as accounted for by Fermi-Dirac statistics. Therefore, this contribution remains manageable in thermoelecric devices under ambient conditions.

The more important contribution to the thermal conductivity is from the lattice. This contribution is more complicated due to the fact that lattice heat transport requires the use of a quasiparticle, the phonon. By using phonons, a theory can be developed regarding the heat capacity of a lattice [21]. Applying the density of phonon states in the material and using the Debye approximation (constant sound velocity in the medium), the following form for the heat capacity results.

$$C_v = 9Nk_b(\frac{T}{\theta_D})^3 \int_0^{x_d} \frac{x^4 e^x}{(e^x - 1)^2} dx \tag{1.6}$$

with $\theta_D(\omega_D)$ being the Debye temperature (frequency) and x_d being defined as $x_d = \frac{\hbar\omega_d}{k_b T}$. An example of a heat capacity curve is shown in figure 2 [2].

The heat capacity is useful, on the basis that an optimized material should support a large temperature gradient, but also respond quickly. As a result, the material should have

[2]figure reproduced with permission of Publisher, John Wiley and Sons

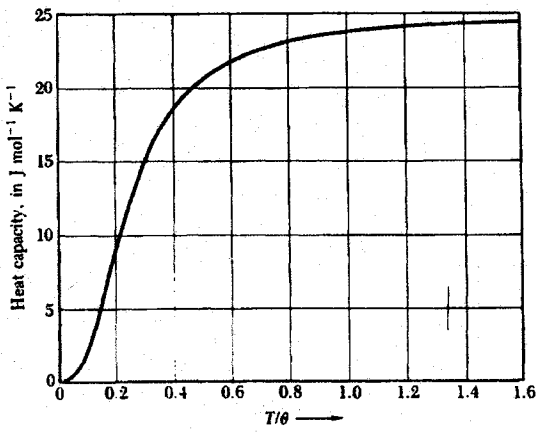

Figure 2 Theoretical Heat Capacity Curve [21]

a low thermal conductivity, which can be achieved through phonon scattering mechanisms. However, it should also have a low response time. This response time would be directly linked to the heat capacity of the lattice. The larger the heat capacity, the slower the response time in the material. As such, a mechanism to cause phonons to scatter in the material, without significantly affecting its heat capacity, needs to be investigated. Unfortunately, there is really nothing that can be done about the electronic contribution to the thermal conductivity, since it is directly tied to the charge carriers (both holes and electrons). Any effect on them will cause a change in the electrical conductivity of the material, which may not be desirable at all.

From all of the previous information, it becomes obvious why this particular field can prove very challenging for basic research. It is remarkably difficult to identify what elements might work well just as basis materials, let alone what to dope them with and how much to achieve the desired effects. So, the goal of this research is to utilize the technique of pressure tuning to learn more about the fundamental structure and abilities of the well established thermoelectric, Bi_2Te_3.

To this end, the project will be presented in the following manner. Chapter 2 will deal with the experimental details and procedure for the experiments. Chapter 3 will present the collected data and compare with previously published results. Finally, Chapter 4 will

summarize the work and results, present some conclusions about the work, and mention some potential future improvements and studies.

CHAPTER 2

EXPERIMENTAL BACKGROUND

The purpose of this chapter is to describe the measurements performed on Bi_2Te_3. This begins with an overview of what pressure tuning is and how it is achieved in the laboratory. To provide a broad view of the techniques used, a brief description of chemical substitution studies will also be presented. Following this, a detailed description of the various experiments is presented. These include x-ray diffraction studies, thermal conductivity and Seebeck coefficient studies, electrical resistivity studies, and heat capacity measurements.

Experimental Techniques

The Achievement of Pressure Tuning The concept of using pressure to tune the parameters of a structure is fairly straightforward and is hardly new. Although there are many different methods for achieving these pressures, the focus for this work is on two of them. These are the Bridgman opposed anvil cell and the diamond anvil cell (DAC).

The basic operating principle is the definition of pressure

$$P = \frac{F}{A} \tag{2.1}$$

where F is the applied force and A is the area it is applied over. Since the maximum possible force is determined by the mechanical properties of the material being used, it becomes necessary to tailor the method to allow a large value for the maximum pressure. This requires that the application area remain small relative to the device used to apply it.

The Bridgman opposed anvil cell consists of two relatively incompressible materials with polished faces (culets) opposing each other. In this application, these anvils are made of tungsten carbide and supported by heat-treated steel binding rings. The sample is contained

within a pressure retaining gasket and placed between the anvils. The pressure is applied by compressing the anvils together.

For this application, the gasket is made of two pieces (Split Gasket Method). The outer annular region is composed of two pyrophyllite annuli (Grade A Silicate Lava, Maryland Lava Company) with an outer diameter of 6 mm, inner diameter of 2 mm, and a thickness of 0.25 mm each. The inner region of each disk has been replaced by the softer mineral steatite (Grade M Silicate Lava, Maryland Lava Company). Two different materials are used due to the fact that pyrophyllite is a stiffer material and better for retaining pressure. However, to minimize shear forces, the sample should be in a quasihydrostatic environment. A diagram of the Bridgman anvil cell is shown in figure 3.

Diamond anvil cells (DAC's) are similar in operation to the Bridgman anvil cell. The anvils, however, are diamonds and the gasket is typically made of a metal, since metals extrude and can retain much higher pressures. In addition, the metallic gaskets are usually filled with a liquid or liquefied gas to provide the desired hydrostaticity and the sample is significantly smaller. A picture of a pair of DAC's is presented in figure 4.

Figure 3 Tungsten Carbide Bridgman Cell

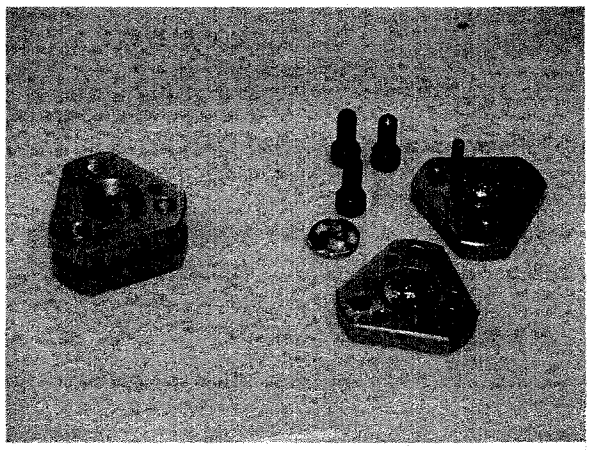

Figure 4 Merrill Bassett Diamond Anvil Cell

Calibration of Pressure in the Bridgman Cell Although the measurements in a large volume Bridgman cell are much easier to do, the typical method of calibrating the internal pressure (ruby fluorescence) cannot be used in this application due to lack of optical access to the sealed pressure chamber. As a result, the pressure inside the Bridgman cell is calibrated using an internal resistive standard. This process will produce data clearly showing the high pressure resistive phase changes as dramatic shifts in the resistance. An example of this is shown in figure 5.

For this study, the internal standards used to calibrate the internal pressure were elemental Bismuth, Tin, and Lead. From NIST measurements of these defined fixed points, measurements of these three metals show resistive phase transitions at 2.55 (Bi I-II), 2.7 (Bi II-III), 7.67 (Bi III-IV), 9.4 (Sn I-II), and 13.4 (Pb I-II) GPa, for the transitions in parenthesis. By preparing the cell in the same method used for the sample, the resistivity vs. pressure can be measured and this data used to calibrate the internal pressure. This produced the calibration data shown in figure 6. As can be seen, the internal pressure of the cell remains fairly linear over the entire region of interest.

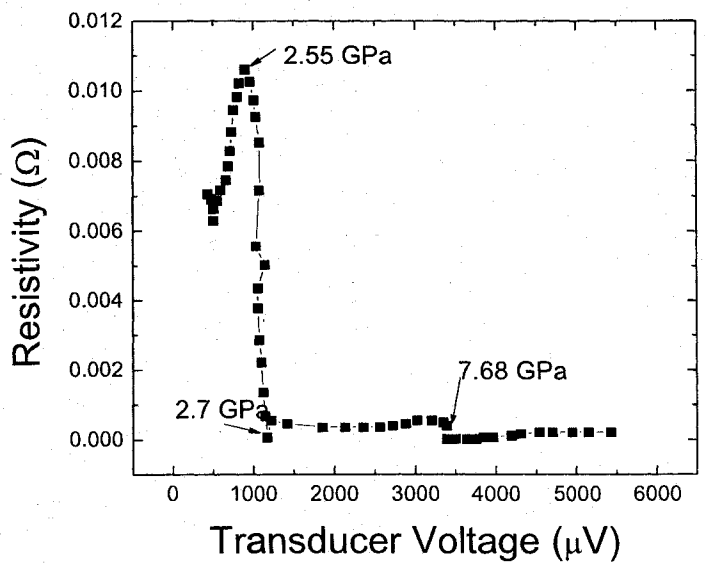

Figure 5 Bismuth Resistive Standard Measurement

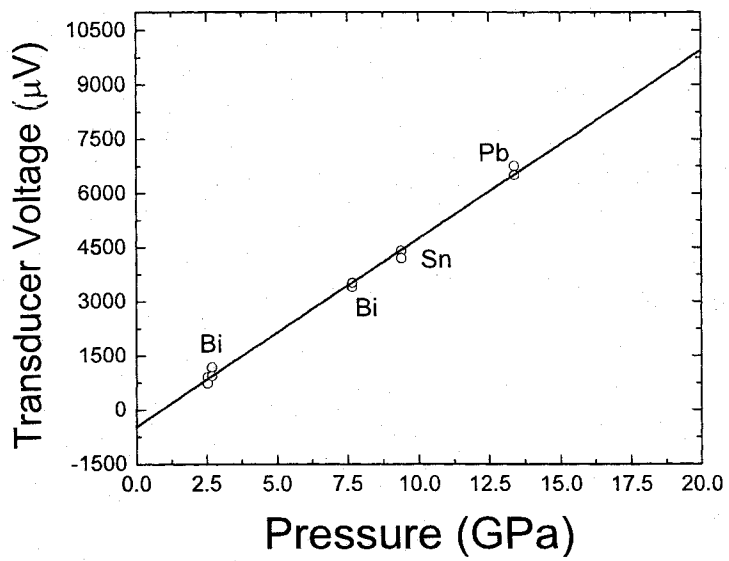

Figure 6 Tungsten Carbide Pressure Calibration Data

In addition, a relation between the measured error at each transition pressure and the pressure it was measured at was determined by inspecting the broadness of each transition and computing the pressure range it corresponded to. Since resistive transitions are typically very sharp, the broadness of the measured transition point gives information about the pressure gradient across the sample. From this, error bars are obtained for each pressure point.

Chemical Substitution The most common method for attempting to improve thermoelectric materials is through the application of chemical substitution. In general, this involves replacing some of one of the elemental constituents with a neighbor in the periodic table. As a brief example of how this works, there has been much effort on studying $Bi_{2-x}Sb_xTe_3$. Applying chemical substitution, the experimenter causes changes in the structure (i.e. cell volume, bond lengths, and possibly structure symmetry) depending upon how much of an element is substituted.

In general, drastic changes in the sample structure can result in the experimenter completely overlooking what was desired. This is caused by the lack of control over the output from a chemical substitution. The target of the above example might be to have $x = .677$ and could result in something less or greater than that. However, it almost never results in the exact stoichiometry that was originally desired. These drastic changes in the structure can, and often do, result in drastic changes in the properties of the material. Whether electrical, thermal, or optical, the properties of the material used may be significantly different from what was intended to be measured as a result of chemical substitutions.

In addition, homogeneity of the sample is a significant issue to address. In chemical substitution experiments, one of the common methods for preparing a sample is to mix the required amounts of raw elements or compounds together and either mill them or melt them together to form the mixture. This commonly results in a very inhomogeneous mixture of the materials. As a result, the experiment performed is not revealing results of the originally intended material, but some inhomogeneous mixture of materials.

It is for this reason that pressure tuning is the technique used in this investigation. Pressure tuning provides more control over the structure of the material under study. In

addition, the changes that are caused to the structure tend to be far less drastic than those resulting from chemical substitution. As a result of this, it becomes much easier to better understand the nature of thermoelectric materials.

Basic Measurements

For a given sample, the typical dimensions in the Bridgman cell are 1.5 x 0.75 x 0.2 mm. The sample used in a DAC is powdered and has a mass of approximately 0.5 μg. The Bridgman cell was used for all the electrical and thermal measurements. All optical measurements were performed using the DAC. Heat capacity studies were performed under ambient pressure in a Quantum Design Physical Property Measurement System (QD PPMS). The applied pressure is determined through the resistance calibration above for the Bridgman cell and the ruby fluorescence method for the DAC. Due to the fact that structural correlations are important to our understanding, x-ray diffraction will be the first topic discussed.

X-Ray Diffraction

Structural studies are important indicators of changes in the properties of a system. For example, the electrical conduction properties depend strongly on the shape of the Fermi surface of a material. This in turn depends upon the shape of the unit cell of the material. As a result, any structural changes alter the shape of the unit cell, thus causing a change in the material properties.

Based upon this, the first set of experiments done regarding Bi_2Te_3 are structural x-ray diffraction measurements. The governing relation for any x-ray diffraction experiment is Bragg's law,

$$\lambda = 2dsin(\theta) \tag{2.2}$$

where λ is the incident wavelength, d is the crystal lattice spacing, and θ is the diffracted angle.

For x-ray diffraction studies, there are two methods for obtaining data. Through the use of Bragg's law, the possibilities are to fix the incident wavelength and measure varied angles (Angle Dispersive X-Ray Diffraction) or fix the measured angle and allow varied

wavelengths/energies through (Energy Dispersive X-Ray Diffraction). Both of these studies were performed in an effort to learn as much as possible about the structure of the material. The basic procedure for these experiments is as follows.

The sample was loaded into one of the previously described DAC's along with a ruby chip and a small amount of a pressurization media. The sample was then placed in the beam path of a focused x-ray source and diffracted to create a Laue ring pattern. Through use of the computer program Fit2D [16], this ring pattern is angularly integrated to give an intensity versus diffraction angle pattern for the sample. Once the pattern is integrated, it can be loaded into a structural analysis program, such as MDI's Jade [32], to analyze the structure and obtain the cell parameters and volume. The pressure in the cell would then be increased and the process done again. These measurements are performed using the synchrotron x-ray source and high pressure diffraction facilities at HPCAT, Sector 16 of the Advanced Photon Source at Argonne National Laboratory, shown in figures 7 and 8. After determination of the cell volumes and lattice parameters, the bulk modulus and pressure derivative are obtained through EOSFit [2], a DOS program for fitting equations of state.

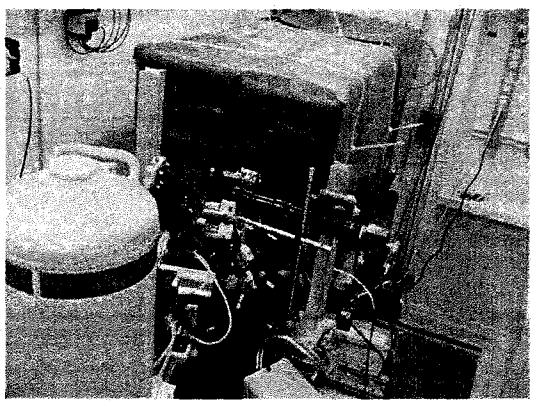

Figure 7 16 BM-D: EDXRD

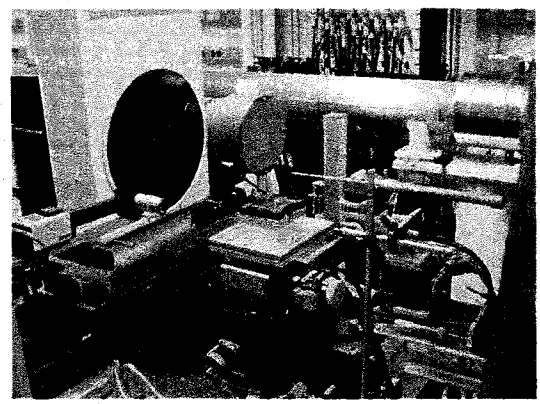

Figure 8 16 ID-B: ADXRD

Electrical Resistivity

The electrical resistivity of a material depends strongly on the conduction of the electrical carriers. Again, referring to the concept of chemical substitution, electrical resistivity is one

of the more common properties modified using small amounts of various elements added to a structure. This type of substitution, termed doping, is quite commonly used to alter the resistivity of a materal.

For the pressure tuning side of this, the goal is more on attempting to alter the band structure of the material subtely by small changes in interatomic spacing and more drastically through phase changes. By altering the band structure, the experimenter can cause electronically allowed levels in the material to migrate towards the Fermi level mentioned in the introduction. In doing this, the the electronic properties are altered and the effect on transport properties can be assertained.

The typical setup for measuring this type of property is a four wire resistance probe. This setup requires the sample to be placed inside the tungsten carbide cell with four leads present to allow for conduction through the sample. The idea is that two of the probes are used for input current, one positive and one negative. Then, the remaining two probes are placed further in along the sample and used for potential difference measurements, again one positive and one negative, as shown in figure 9[1].

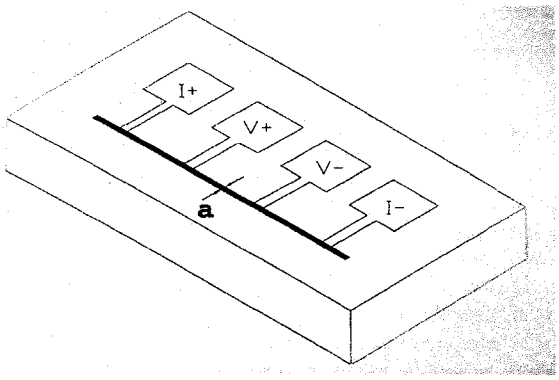

Figure 9 Diagram of Resistivity Measurements [34]

In addition, the polarity of the current leads is switched in an AC fasion to remove any residual resistance effects. This polarity switching is required to eliminate effects, such as the Hall effect or thermal voltages, from causing anomalous resistance readings. Also, by adding the two leads, contact resistances can be removed, as long as all four leads are connected in

[1]figure reproduced with permission of Publisher, Springer Verlag

the same manner.

After completion of the calibrant samples, mentioned earlier, two Bi_2Te_3 samples were prepared with sample dimensions of approximately 1.50 mm x 0.37 mm x 0.10 mm. These samples were placed in a carved recess in the lower steatite gasket and four copper leads were laid across the sample in grooves carved in the pyrophyllite gasket. With this setup, the data was collected through a Lakeshore Model 370 resistance bridge with an excitation current of 10 mA. The device was set in constant current mode and computes the resistance through use of the relationship $P = I^2/R$. The data was collected in a range from $\approx$ 1 GPa to 18 GPa, with pressure computed from a transducer voltage using the calibration previously determined.

Thermal Conductivity and Seebeck Coefficient

As discussed earlier, the main method of heat transport in a non-metallic lattice is through phonons. The ability of a phonon to conduct heat is determined, in part, by the number of energy quanta it carries and the mean free path for phonons in the structure. Although little can be done regarding the contained energy, the mean free path can be greatly changed. This path length is the average distance a phonon can travel without colliding with something(a defect, boundary, or other scattering center). The obvious idea is to minimize the path length by scattering the phonons often.

To begin with, the traditional method for measuring the ambient pressure thermal conductivity is to place the sample between two pieces of material with known good thermal conductivity. One of these is used as the heat source and the other as the heat sink. The material under study is then exposed to a temperature gradient. The thermal conductivity is measured by varying the temperature gradient and measuring how much heat passes through the sample from the source to the sink, as shown in figure 10[2].

This method for measuring thermal conductivity is also remarkably useful for performing Seebeck coefficient measurements. Since the Seebeck coefficient also depends on a temperature gradient, by simply welding or fixing the thermocouples used for measuring the temperature difference to the sample, a potential drop can be measured between the leads of

[2]figure reproduced with permission of Publisher, Springer Verlag

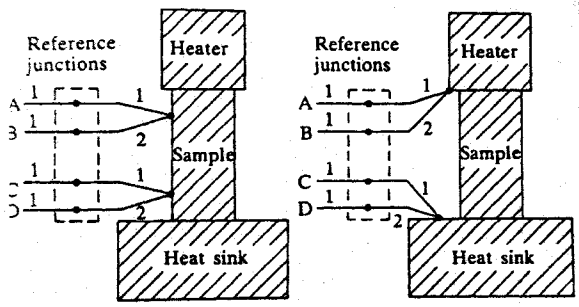

Figure 10 Diagram of Thermal Conductivity Measurements [34]

the two thermocouples. This allows the determination of the thermal conductivity and the Seebeck coefficient simultaneously.

The process used for measuring these properties at high pressure is similar to the method used for the electrical resistivity measurements. The samples were cut to size and placed in a carved recess in the lower steatite gasket. Then, a matched pair of thermocouples (Type K: Alumel-Chromel) were laid across the sample ends with a manganin heater wire laid in a groove at one end of the sample. The thermocouples were fixed to the sample using gold paste to ensure conduction through the sample and a more accurate thermal measurement. The loading looked similar to that shown in figure 11.

Figure 11 Thermal Conductivity and Seebeck Coefficient Setup

This type of setup requires a different method of measurement depending on the samples ambient thermal conductivity. For samples with a thermal conductivity much larger than

the thermal conductivity of the gasket material ($\lambda_{sample} >> \lambda_{gasket}$), it conforms with a method called the short hot wire method. In this method, the heat coupled into the sample is conducted directly along the sample and very little is radiated perpendicular to the propagation direction due to the large differences in thermal conductivities. This results in lower errors, but tends to be less applicable at high pressures. For samples with thermal conductivities on the order of the gasket thermal conductivity ($\lambda_{sample} \approx \lambda_{gasket}$), this setup produces a guarded hot wire style technique, which occurs when the sample radial heat loss is low due to the material around it having a similar temperature profile. This setup tends to have larger errors due to a larger radial heat loss. However, it tends at be applicable to much higher pressures.

In addition to the different types of measurement methods that the designed setup applies, there are two other typical methods for measuring the thermal conductivity. The first method is called the transient or 3ω method. This method applies an AC heat source to the sample and measures the decay time of a temperature pulse to compute the thermal conductivity of the sample. The other method, used for these measurements, is the steady state heat flow method. The temperature gradient is increased and held steady at the maximum temperature to measure the thermal conductivity. These regions of interest are shown below in figure 12. The steady state method was chosen because it is easier to setup and provides more data points for determination of the thermal conductivity.

The measurements were taken by pressurizing the cell to a particular pressure, typically one GPa steps. At each pressure point, current through the heater wire was increased, dissipating approximately four watts of power across its length. After two minutes with the heater on, it was slowly turned off and the system allowed to cool. Then, this process was repeated two more times before increasing to the next pressure point.

By knowing the output power, the amount of emitted radiation coupled directly into the sample can be calculated from the geometry of the situation and its experimental specifics. Also, knowing the sample dimensions and measuring the temperature drop across the sample,

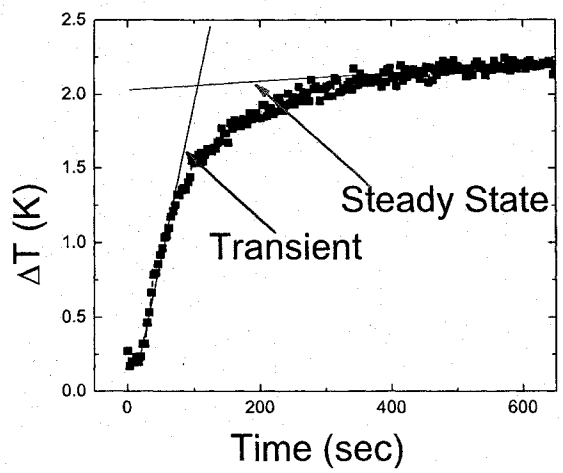

Figure 12 Thermal Conductivity Measurement Method Regions

the thermal conductivity can be calculated using

$$\lambda = \frac{\gamma V I}{A} \frac{\delta x}{\delta T} \tag{2.3}$$

where λ is the thermal conductivity, γ is the coupling factor (more detail in paragraph below), V is the potential drop across the heater, I is the current through the heater, A is the sample area perpendicular to the flow of heat, δx is the distance between the thermocouple junctions, and δT is the temperature difference between the thermocouples.

Since the thermocouples are fixed to the sample at two locations, the Seebeck coefficient is measured by determining the potential drop between the two chromel wires of the individual thermocouples. Several papers mention different methods for measuring the Seebeck coefficient. [5], [48] However, after much consideration, it seemed that the easiest way was by a direct measurement of the potential drop. By using the two chromel wires, any contact Seebeck effect between the thermocouple wires and the sample will be undone, since it is safe to assume similar contact conditions. Thus, the Seebeck coefficient is determined in the manner presented in chapter 2,

$$\alpha = \frac{\delta V}{\delta T} \tag{2.4}$$

Calculation of γ For ease of experiment and calculation, the heater wire was placed against one end of the sample. From this, assuming that the heat is emitted uniformly in all directions, only the emitted radiation components that are along the length of the sample will be coupled and flow in the manner needed to be measured. From this, the overall resistance of the heater wire is measured, and with the resistivity of the heater material known, the resistance of the segment directly coupled to the sample can be calculated.

For these experiments, the ratio of the sample heater resistance to the overall heater resistance is on the order of .0001. Furthermore, only about $\frac{1}{3}$ to $\frac{1}{4}$ of the emitted radiation is coupled into the sample surface at all, and only about $\frac{1}{2}$ of that is along the sample transmission direction. As a result, γ is typically on the order of 10^{-5}.

Although this coupled power seems small, the ideal situation for thermal conductivity measurements is to have as little measureable change in the overall temperature of the sample as possible. This way, our uncertainty in the temperature of the measured thermal conductivity is minimal. However, it is also desireable to have a large temperature gradient across the sample. As a result, there are several tradeoffs required to ensure that the thermal conductivity measured is accurate and at the temperature desired.

Heat Capacity

Although heat capacity is not a required parameter for the determination of anything thermoelectric about the material, as was discussed in the introduction, it can effect the response time of the thermoelectric material. The higher the heat capacity is, the longer it takes for the sample to "feel" the temperature gradient across it. As a result, it takes far longer for the Seebeck effect to take hold and begin to generate useful current.

In addition to this, heat capacity is often a quantity used to verify phase transitions in the structure of a material or for information regarding the thermal conductivity. Due to this, it was included for the potential use in these areas and to ensure that all possible thermal characterizations available are performed on the sample. Also, there are several useful quantities related to the heat capacity that can be derived from this data. For example, the enthalpy of the material can be obtained by doing a simple integral over temperature of

the measured heat capacity.

$$\Delta H = \int C_p \, dT \tag{2.5}$$

For this work, the heat capacity was measured under ambient pressure and varying temperature to get an idea of how responsive Bi_2Te_3 is as a thermoelectric. This measurement was done using the Physical Property Measurement System (PPMS), developed by Quantum Design. The basic idea of this measurement is as follows.

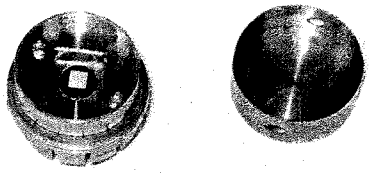

Figure 13 PPMS Heat Capacity Puck

A small pellet of the sample material is made and set aside. The PPMS system is equipped with small sample pucks designed for specific measurements. In this case, the heat capacity puck, as shown in figure 13, is composed of the outer housing, four pairs of electrical leads, and a sample pad. The sample pad is first covered with a thin layer of thermal grease, either Apiezon© Brand N or H grease. Then, a temperature range identical to the desired measurement region is measured using just the sample stage and grease, with no sample present, to produce an addendum. Subtraction of the addendum allows a determination of the sample's heat capacity. Following this run, the sample is inserted into the system and the data is collected. Now that the measurement processes have been described, the results of this study can be presented, as they are in the next chapter.

CHAPTER 3

RESULTS AND DISCUSSION

The goal of this chapter is to present the data collected on Bi_2Te_3 and to provide comparisons with results from previously published work. The format will be similar to the previous chapter, discussing the results of each individual experiment.

Structure Results

The high pressure x-ray diffraction performed on this compound yielded some unexpected results regarding the structure of Bi_2Te_3. Previous work on this material using resistivity studies under pressure [46] displayed the possibility for two phase transitions in the physical structure between ambient pressure and 10 gigapascals (GPa) [1]. These phase transitions were reported to occur at approximately 6.8 GPa and 8.2 GPa at ambient temperature. The ambient crystal structure of Bi_2Te_3 is shown in figure 14.

The initial structure of Bi_2Te_3 is in the rhombohedral $R\bar{3}m$ structure with parameters as shown in table 1. Through the measurements made at HPCAT, it was found that Bi_2Te_3 undergoes two phase transitions in the pressure region between ambient and approximately 23 GPa. A selection of the diffraction patterns is presented in figures 15 and 16. In the diffraction patterns, the bottom pattern has x-ray fluorescence peaks for the individual elements marked. These peaks were excluded during the data analysis.

[1] 1 GPa = 10 Kbar

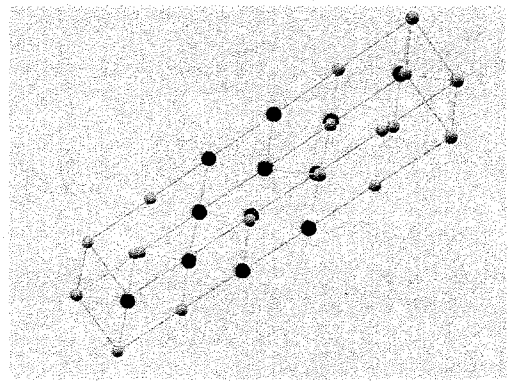

Figure 14 Crystal Structure of Bi_2Te_3

The first transition was found to begin around 7.2 GPa and complete around 9.7 GPa. This transition was a structural change from the ambient rhombohedral group to the orthorhombic space group I222, whose parameters are also shown in table 1. This transition is of particular interest due to the fact that the pressure region where the phase transition occurs corresponds well with the electrical resistivity data previously collected on this material. [46]

Table 1 Derived Cell Parameters

Parameter	R$\bar{3}$m	I222
a (Å)	4.386 (1)	11.66(1)
b (Å)	4.386 (1)	4.819 (1)
c (Å)	30.46 (1)	7.467 (1)

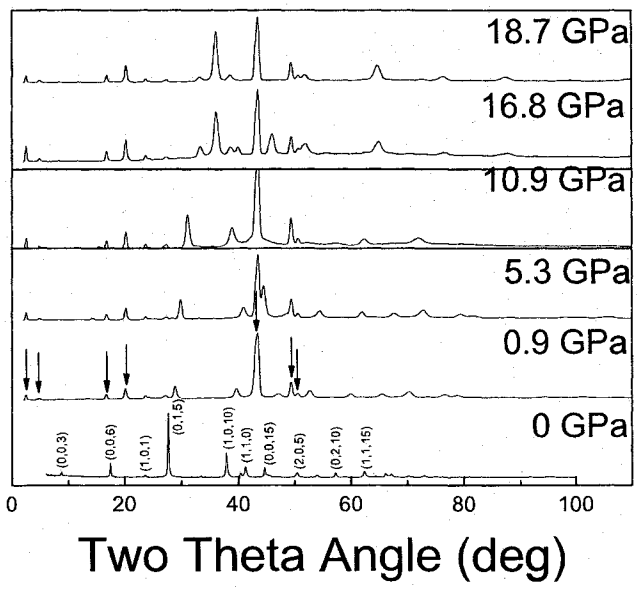

Figure 15 Compression Patterns

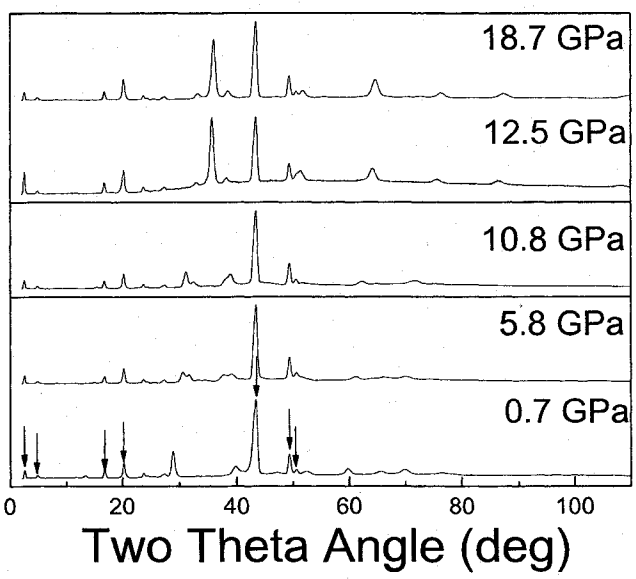

Figure 16 Decompression Patterns

Following this, the structure remains in the I222 space group up until approximately 16 GPa, when it undergoes a transition to another orthorhombic space group, Iba2. This phase transition is accompanied by a change in the molecules per unit cell from three to one. A graph of the volume versus pressure is presented in figure 17. It should be noted in this graph that the volume of the third phase (Iba2) has been multiplied by three to make it comparable to the volumes of the previous two phases and there was evidence of this phase appearing around 14 GPa. However, there was not a sufficient number of distinct peaks to determine a cell volume for this phase until 16 GPa.

The information in table 2 entailed fitting the data to a third order Burch-Murnaghan equation of state. These fits are the lines in figure 17. This equation of state has the form

$$P(V) = \frac{3B_0}{2}[(\frac{V_0}{V})^{\frac{7}{3}} - (\frac{V_0}{V})^{\frac{5}{3}}](1 + \frac{3}{4}(B_0' - 4)[(\frac{V_0}{V})^{\frac{2}{3}} - 1]) \tag{3.1}$$

with the derived cell data presented in table 2 below. In this equation, V is the measured volume at pressure P, V_0 is the ambient pressure volume, and B_0 is the ambient pressure bulk modulus.

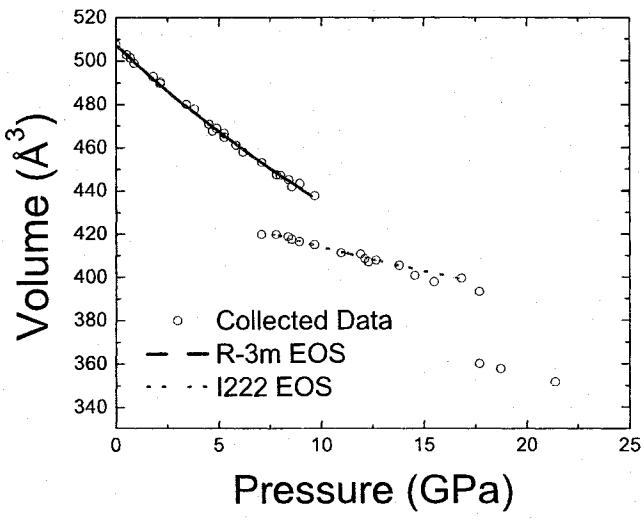

Figure 17 Bi_2Te_3 Compression P vs. V

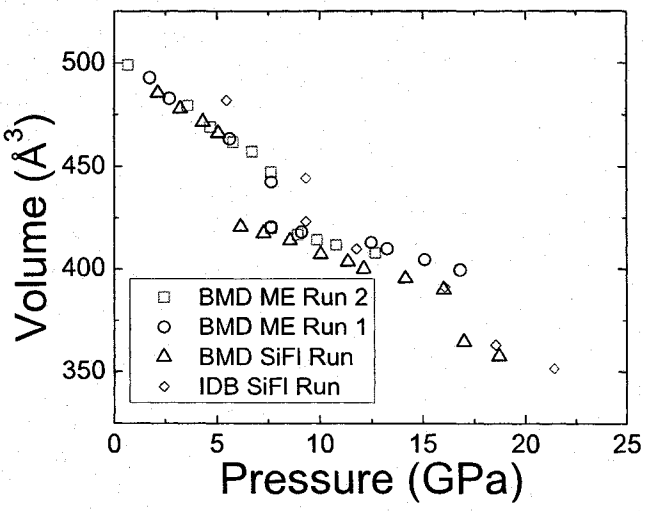

Figure 18 Bi_2Te_3 Decompression P vs. V for four experiments

Table 2 Derived Cell Data

Parameter	$R\bar{3}m$	I222
V_0 (Å^3)	507.5(1)	445(2)
B_0 (GPa)	2.1 (3)	6

In addition to the compression data, the sample was exposed to x-rays during the decompression process. This demostrated that the sample reverted to its original state under release of pressure. A plot of the volume versus pressure for the decompression cycle is presented in figure 18.

In the decompression plot, it should be noted that the data do not show the same consistency as they do during compression. This effect has been studied by several groups and is due to the different pressure media used for the experiments. Recent research by Shen *et.al.* [44] and Ragan *et.al.* [40] shows that over the pressure range from zero to eight and 16+ GPa, silicone fluid shows behavior that is more favorable for application as a pressure medium over the methanol:ethanol mixture. In contrast, silicone fluid has been shown, by similar comparisons, to not be as desireable in the region from 8-16 GPa. For comparison with the previously mentioned resistivity data, it was determined that the next step should

be to test the electrical resistivity of the sample under pressure.

Electrical Resistivity

As was mentioned in the previous section, the electrical resistivity of Bi_2Te_3 was previously measured up to 8.5 GPa by Vereshchagin *et. al.* [46] In their results, they demonstrated that the resistivity shows dramatic decreases around 7-8 GPa. From this information, it was expected that our sample would show similar behaviour. This also correlates well with the previously measured x-ray diffraction data. The collected data is shown in figure 19.

In the beginning, there is a sharp rise in the electrical resistance up to 3 GPa. Following this, the resistance decreases and shows reproducible, sudden drops in the sample resistance occurring between 6-6.5 GPa, 13-14 GPa, and 15.5 GPa. These three transitions match well with the structural data collected earlier for the Bi_2Te_3 I-II, beginning of II-III, and end of II-III transitions.

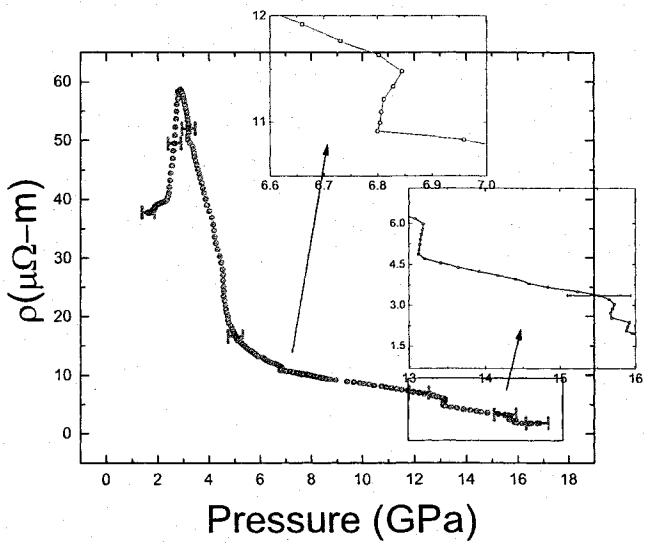

Figure 19 Bi_2Te_3 Resistivity vs. Pressure

Of additional interest is the drop in the resistance that occurs around 4.5 GPa. This drop was also reported previously in Vereschchagin *et.al.*'s work. At the time, they attributed this particular drop to a phase transition in the structure of the material. However, as was seen

in the x-ray work presented here, this does not seem to be the case. A possible explaination for this will be discussed in the final section of this chapter.

Thermal Conductiviy and Seebeck Coefficient

Seebeck coefficient: The Seebeck coefficient of Bi_2Te_3 has been previously measured at ambient conditions by several researchers including Goldsmid[12], Charles[6], and Mansfield[29]. Unfortunately, these values tend to vary significantly depending upon contact and surface conditions. However, the typical ambient range reported in literature for the Seebeck coefficient α lies in the range from 65-200 $\frac{\mu V}{K}$ and depends strongly on impurity concentrations.

Using the setup described in the previous chapter, the Seebeck coefficient was measured by using thermocouples to determine the absolute temperature at two points on the sample and measuring the potential drop between the chromel wires of these two thermocouples. Through this method, the data collected is shown in figure 20.

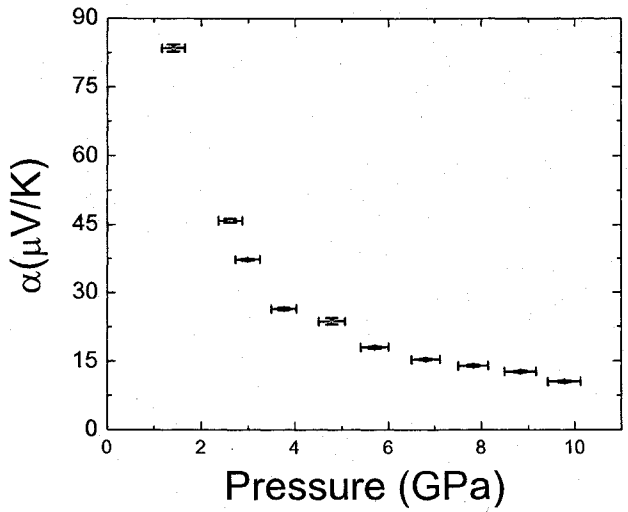

Figure 20 Bi_2Te_3 Seebeck Coefficient vs. Pressure

As can be seen in this data, the Seebeck coefficient of Bi_2Te_3 is dramatically reduced through the application of pressure. Extrapolation of the curve to ambient conditions produces a value for the ambient seebeck coefficient of approximately 175 $\frac{\mu V}{K}$, which lies well within the previously reported range for the material at ambient pressure and agrees well with our measured value under ambient conditions. The trend under pressure seems to follow

a similar trend to the resistivity, discussed in the previous section. It should be noted that the Seebeck coefficient displays no evidence of the phase transition found to occur around 8 GPa. In addition to this, there is a small shoulder that appears in the data around 4.5 GPa that should be noted by the reader. This will be discussed in the final section of this chapter.

In general, this corresponds well with previous knowledge for this type of measurement. One would expect that as pressure is applied to the rhombohedral structure of Bi_2Te_3, the Seebeck coefficient would decrease. In work done by Larson *et.al.*, the calculated density of states for the material shows a large density of states near the Fermi surface with some states actually touching the Fermi surface of the material at ambient pressure. As pressure is applied to this material, one would expect the states touching the Fermi surface to begin to shift above it, as shown by Jaros *et.al.* [19] and Bartkowiak *et.al.* [4]. This shift would allow more electrons into the conduction band and reduce the overall potential drop across the material significantly. In addition, the measured change in the thermal conductivity, as shown in the next section, does not change enough to significantly affect the thermal gradient across the sample. As a result the change in potential drop across the sample falls and the Seebeck coefficient falls in direct proportion to this parameter.

Thermal Conductivity: The thermal conductivity of Bi_2Te_3 was also measured by Goldsmid[12] at ambient pressure, with a value of $\lambda = 2.44\frac{W}{mK}$. For this experiment, the sample preparation was performed in the same manner as the Seebeck coefficient measurements. This experiment yielded the results shown in figure 21.

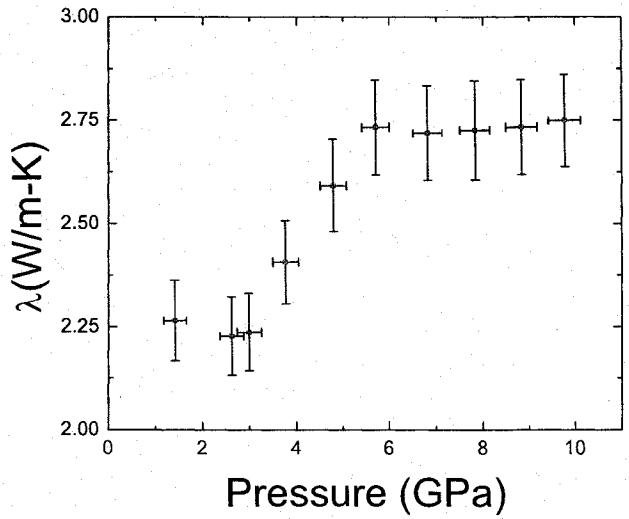

Figure 21 Bi_2Te_3 Thermal Conductivity vs. Pressure

In this figure, it should be noted that the thermal conductivity of the sample increases with pressure. This correlates well with what would be expected to occur. If the Fermi surface were to increase in size rapidly, as would occur with the compression of the material, increasing the phonon frequencies allowed to propagate in the lattice. This will result in a larger heat transport through the lattice. It should also be noted that in the 7-8 GPa range, the sample shows a stabilization of the thermal conductivity. As the Fermi surface levels off, as might occur through a reorientation or restrucutring of the unit cell, the increase in the phonon frequencies will stop as well. This will require that no more frequencies be added to the phonon modes in the lattice and the thermal conductivity through the lattice will level off. Using a similar explaination, it is possible that the initial decrease in the thermal conductivity is due to the destruction of phonon modes from the initial compression of the material.

Heat Capacity

In order to make a more complete set of thermodynamic measurements, the heat capacity of Bi_2Te_3 was measured over the temperature range from 1.8 K to 350 K. Before going on, it should be noted that the Debye model used for fitting the data is computing a constant

volume heat capacity C_v. In contrast, the PPMS heat capacity measurements are done at constant pressure, C_p. As a result, there is a necessary conversion between these two heat capacities using the equation [47]

$$C_p - C_v = \frac{TV\alpha^2}{\beta_T} \tag{3.2}$$

with T being temperature, V being volume, α being the volumetric thermal expansion, and β being the isothermal compressibility. For this conversion, the temperature is measured, and β is determined by inverting the zero pressure bulk modulus obtained from x-ray diffraction. The volume is dependent upon α and, as such, is calculated at each temperature using the α values obtained from literature.[10],[31]

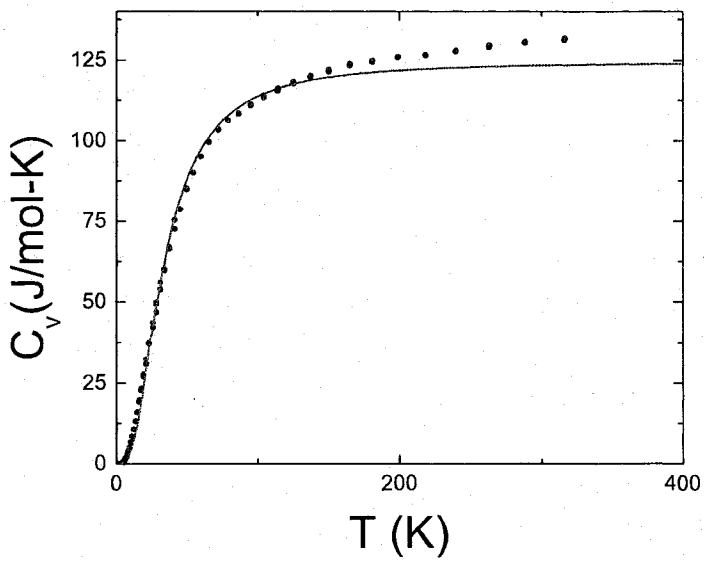

Figure 22 Bi_2Te_3 Heat Capacity

From this fit, presented in figure 22, it was determined that the Debye model does not account for the entirety of the measured heat capacity values. In an effort to account for this, several possibilities for the discrepancy were investigated. First, it was found that by considering the internal vibrations to be accounted for using an Einstein approximation, a decent fit to the data was obtained. This only occured for the combination mode from all

of the possible infrared and raman modes, with a total wavenumber of 563 cm^{-1}. [22]

Another possibility to explain this is that there is a high temperature electron contribution to the heat capacity that is not accounted for in the Debye model. This contribution could be included by doing a low temperature fit to the data of the form $C_{p,lowT} = \gamma T + \beta T^3$. This yielded a reasonable fit, with $\gamma = 0.021 \frac{J}{molK}$ and $\beta = .0061 \frac{J}{molK^4}$. In this form, the γ term would account for the electronic contribution to the heat capacity. By adding this term back on, it was found that a decent fit was obtained for the presented data. This demonstrates that there is some electronic part of the heat capacity for this material, as γ would be zero if there were no heat capacity in the electrons. For these three setups, the Debye temperature Θ_D was found to have the values 137.3 K, 138.3 K, and 140.2 for the Debye model alone and with both Einstein and electronic corrections, respectively. In addition, previous reported results from Gorbachuk *et.al.* [13], shown below in figure 25, compares well with our measured data for the region between 75 and 300 K.

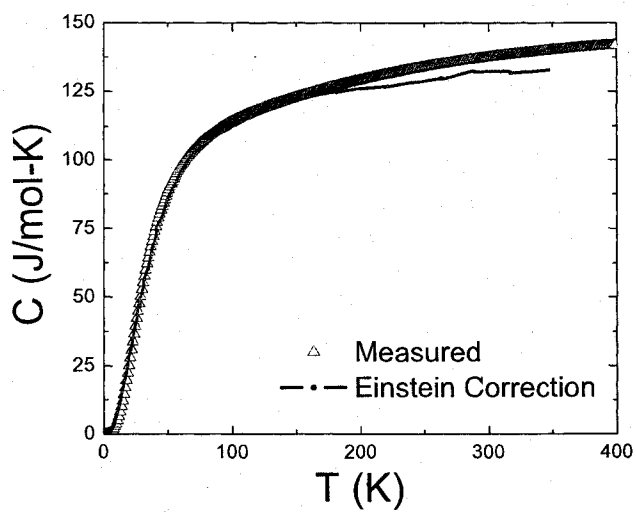

Figure 23 Einstein Correction

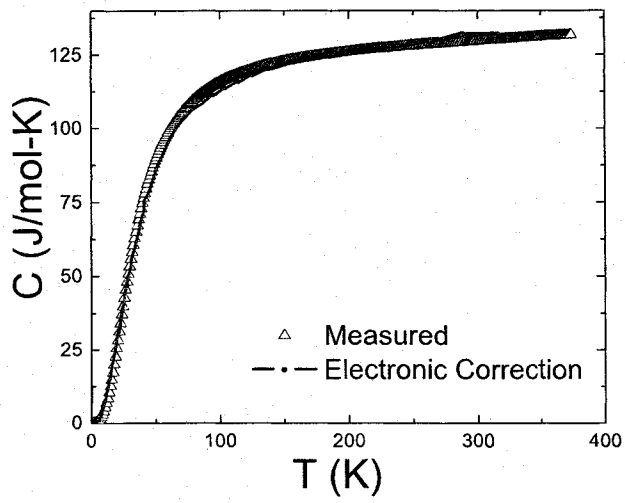

Figure 24 Electronic Correction

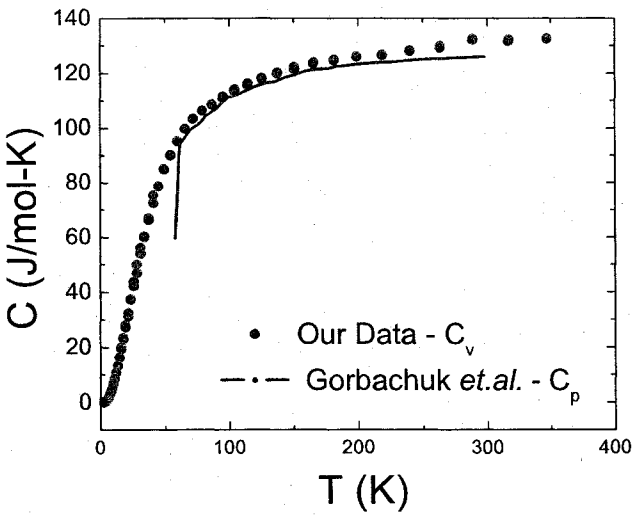

Figure 25 Gorbachuk Heat Capacity vs. Our Data

Electronic Topological Transition?

One of the more common phenomena that occur in materials with special properties, such as superconductivity and thermoelectricity, is the occurance of an electronic topological transition (ETT). This type of transition is actually a restructuring of the Fermi surface of the material and can be induced through low temperatures, magnetic fields, or pressure. In most reported occurances of this type of transition [11],[35],[39] the evidence presented clearly shows that it happened. This has been theorized by Larson *et.al.* [25] and reportedly measured by Itskevich *et.al.* [18] to occur in Bi_2Te_3 under pressure. The report presented by Itskevich studies p-doped Bi_2Te_3 under pressure and shows dramatic evidence in support of an ETT in the doped system. However, aside from theoretical evidence from Larson, there has not been any report of a measurement of an ETT in the pure undoped material under pressure.

Looking back at the data presented in the previous sections, the Seebeck coefficient shows a small shoulder occuring around 4.5 GPa and the resistivity shows a corresponding drop in the resistance. As such, it is possible that the measured data presented hear demonstrates some evidence of the reported ETT for Bi_2Te_3. To further bolster this argument, the work presented by Novikov *et.al.* [35] suggests that that this type of transition would also show evidence through a phonon softening in the material. This would show up in the thermal conductivity as a levelling off or decrease in the measured value as the transition occured. As such, there seems to be some evidence of this type of transition present in the measured data.

CHAPTER 4

CONCLUSIONS

The data presented here helps to better understand the properties of Bi_2Te_3 and what causes changes in them. From the structural information, it has been determined that this material undergoes two phase transitions around 7 GPa and 16 GPa. In addition, these transitions are observable in the resistance data, showing that the materials electrical properties change quite drastically along with the structure. Furthermore, the studies under pressure show an increase in the thermal conductivity and a decrease in the Seebeck coefficient. From this data, a calculation of the ZT parameter has been performed. This information is presented below in figure 26. The first data point is the computed value from ambient pressure measurements. In this diagram, the zero pressure value for ZT was .0404. This value lies well within the range reported previously for Bi_2Te_3. From Goldsmid's data [12], a range from .12 to .013 was typical for various slight dopings and undoped forms of Bi_2Te_3.

Through the use of pressure tuning of the structure of Bi_2Te_3, this study has determined that the overall thermoelectric potential of this material drastically decreases with the application of pressure. However, it does not seem that the changes in the thermal related properties are affected by the previously mentioned phase transitions. This is not intuitive from references on similar compounds. For example, work done on As_2Te_3 by Scheidemantel *et.al.* [43] shows that there is a structural transition in the material occuring around 8 GPa to the Bi_2Te_3 structure. This structural transition also corresponds well with a significant measured deviation in the Seebeck coefficient.

Although this study did not succeed in improving the thermoelectric figure of merit of Bi_2Te_3, it did provide several useful pieces of information. First, the lattice structure of the this material strongly determines the electrical properties. As was presented, Bi_2Te_3 began in a rhombohedral space group and transformed to an orthorhombic space group with pressure

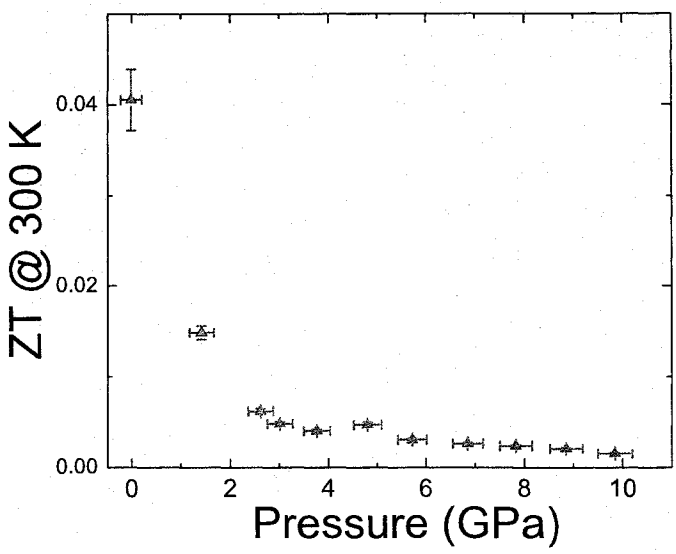

Figure 26 ZT vs. Pressure for Bi_2Te_3

application. The thermal properties, on the other hand, give evidence showing no correlation with the structure. The thermal conductivity seemed to increase with application of pressure and plateaued just before the phase transition. The continuous drop of the Seebeck coefficient is, however, expected for this material. There is evidence in the measured data supporting the reported electronic topological transition in Bi_2Te_3 under pressure, reported by Larson *et.al* [25]. However, this evidence is not conclusive and more studies need to be done to determine if what was seen is truly an ETT.

Overall, it can be concluded that a negative pressure effect on the structure of Bi_2Te_3 might positively effect the thermal properties and might be of interest. This would require a more open structure than the starting structure, or use of larger atoms in place of the constituents of Bi_2Te_3. One could also begin to dope the material slightly to improve the resistivity of the material and the thermal properties somewhat.

Further Work

The next step in this type of study would be to investigate the other typical constituents of room temperature thermoelectric materials, Sb_2Te_3 and Bi_2Se_3, as well as solid solutions of the three. In addition, further development of the thermal measurements at high pressure is planned including the possibility of changing the inner pressure medium to something with a much lower thermal conductivity to improve data quality. This could be accomplished by switching to a Silica Aerogel or something with a similar conductivity. Also, attempts to use a conductive epoxy on the samples for resistive measurements would potentially improve this data quality.

In addition to the room temperature work, it would be beneficial to develop techniques for measuring these parameters under pressure as a function of temperature as well. This is also suggested in the work mentioned earlier by Polvani *et.al.* [39]. They mention in their results that there is a measured sharp maximum in the Seebeck coefficient of doped Bi_2Te_3 around liquid helium temperatures. This type of measurement would help to reveal any ETT's that may occur.

While only intended as an overview of future work, studies on other thermoelectric materials would be of significant interest. This would expand the realm of materials into the more recent skutterudite and clathrate materials, as well as superlattice structures. In addition, it would be of great interest to attempt to dope Bi_2Te_3 to stretch the lattice and see what effect that has on the thermoelectric properties. Current interest in these materials, combined with the measurements performed here, could begin to give us new insights into the workings of thermoelectric materials.

REFERENCES

[1] Andersson, G., Sundqvist, B., and Backstrom, G. *A high-pressure cell for electrical resistance measurements at hydrostatic pressures up to 8 GPa: results for Bi, Ba, Ni, and Si.* Journal of Applied Physics **65**, 3943-3950 (1989).

[2] Angel, R. *EOSFit: Least Squares Equation of State Fitting Software.*

[3] Atkins, P. *Physical Chemistry.* 6^{th} Ed, W.H. Freeman and Co, 1978.

[4] Bartkowiak, M., and Mahan, G.D. *Electronic Structure of Sb_2Te_3 under pressure.* 18^{th} International Conference on Thermoelectrics (ICT), 1999.

[5] Boffoue, O., Jacquot, A., Dauscher, A., Lenoir, B., and Stolzer, M. *Experimental setup for the measurement of the electrical resistivity and thermopower of thin films and bulk materials.* Review of Scientific Instruments, **76**, 053907 (2005)

[6] Charles, E., Groubert, E., and Boyer, A. *Structural and electrical properties of bismuth telluride films grown by the molecular beam technique.* Journal of Materials Science Letters, **7**, 575-577 (1988).

[7] Chen, G., Dresselhaus, M.S., Dresselhaus, G., Fleurial, J.-P., and Caillat, T. *Recent developments in themoelectric materials.* International Materials Reviews, **48**, 45-66 (2003).

[8] da Silva, L., Kaviany, M., and Uher, C. *Thermoelectric performance of films in the bismuth-tellurium and antimony-tellurium systems.* Journal of Applied Physics, **97**, 114903 (2005).

[9] Dheepa, J., Sathyamoorthy, R., Velumani, S., Subbarayan, A., Natarajan, K, and Sebastian, P.J. *Electrical resistivity of thermally evaporated bismuth telluride thin films.* Solar Energy Matreials and Solar Cells, **81**, 305-312 (2004).

[10] Francombe, M.H. *Structure-cell data and expansion coefficients of bismuth telluride.* British Journal of Applied Physics **9**, 415-417 (1958).

[11] Garg, A.B., Godwal, B.K., Meenakshi, S., Modak, P., Rao, R.S., Sikka, S.K., Vijayakumar, V., Lausi, A., and Bussetto, E. *Electronic topological transition in AuX_2 (X = In, Ga, and Al) compounds at high pressures.* Journal of Physics: Condensed Matter, **14**, 10605-10608 (2002).

[12] Goldsmid, H.J. *The thermal conductivity of Bismuth Telluride.* Proc. Phys. Soc., **69**, 203-209 (1956).

[13] Gorbachuk, N.P., Bolgar, A.S., Sidorko, V.R., and Goncharuk, L.V. *Heat Capacity and Enthalpy of Bi_2Si_3 and Bi_2Te_3 in the temperature range 58-1012 K.* Powder Metallurgy and Metal Ceramics **43**, 284-290 (2004).

[14] Goossens, M., Mittelbach, F., and Samarin, A. *The LaTeX Companion.* Addison Wesley, 1994.

[15] Gray, P. *The Dynamic Behavior of Thermoelectric Devices.* John Wiley and Sons, 1960.

[16] Hammersley, A. *Fit2D: Image Plate Conversion Software*, copyright 1987-2005.

[17] Holzapfel, Wilfried B. *Refinement of the ruby luminescence pressure scale.* Journal of Applied Physics, **93**, 1813-1818 (2003).

[18] Itskevich, E.S., Kashirskaya, L.M., and Kraidenov, V.F. *Anomalies in the low-temperature thermoelectric power of p- Bi_2Te_3 and Te associated with topological electronic transitions under pressure.* Semiconductors, **31**, 276-278 (1997).

[19] Jaros, M., Brown, L.D.L., and Morrison, I. *Band structure efects in III-V superlattices under hydrostatic pressure as a means of determining microscopic signature of perfect and imperfect semiconductor interfaces.* Semiconductor Science and Technology, **6**, 417-421 (1991).

[20] Kim, Miyoung, Freeman, A.J., and Geller, Clint B. *Screened exchange LDA determination of the ground and excited state properties of thermoelectrics: Bi_2Te_3.* Physical Review B **72**, 035205 (1-3) (2005).

[21] Kittel, C. *Introduction to Solid State Physics.* John Wiley and Sons, 1996.

[22] Kullmann, W., Geurts, J., Richter, W., Lehner, N., Rauh, H., Steigenberger, U., Eichhorn, G., and Geick, R. *Effect of Hydrostatic and Uniaxial Pressure on Structural Properties and Raman Active Lattice Vibrations in Bi_2Te_3.* Physics of Statistical Solids B, **125**, 131-138 (1984).

[23] Kullmann, W., Rauh, H., Geick, R., Steigenberger, U., and Kuhs, W.F. *Thermal Parameters and Probability Density Functions of the Narrow Gap Semiconductor Bi_2Te_3 under Hydrostatic Pressure* Physics of Statistical Solids B, **148**, 445-455 (1988).

[24] Khvostansev, L.G., Orlov, A.M., Abrikosow, N.K., Svechnikova, T.E., and Chizhevskaya, S.N. *Thermoelectric Properties and Phase Transitions in Bi_2Te_3 under Hydrostatic Pressure up to 9 GPa and Temperature up to 300 C* Physics of Statistical Solids A, **71**, 49-53 (1982).

[25] Larson, P., Mahanti, S.D., and Kanatzidis, M.G. *Electronic structure and transport of Bi_2Te_3 and $BaBi_2Te_3$.* Physical Review B, **61**, 8162-8171 (2000).

[26] Li, Che-Yu, Ruoff, A.L., and Spencer, C.W. *Effect of Pressure on the Energy Gap of Bi_2Te_3.* Journal of Applied Physics **32**, 1733-1735 (1961).

[27] Lundegaard, L.F., Makovicky, E.E., Boffa-Ballaran, T., and Balic-Zunic, T. *Crystal Structure and cation lone electron pair activity of Bi_2S_3 between 0 and 10 GPa.* Physics and Chemistry of Materials **32**, 578-584 (2005).

[28] Lundegaard, L.F., Miletich, R., Balic-Zunic, T., and Makovicky, E. *Equation of state and crystal structure of Sb_2S_3 between 0 and 10 GPa.* Physics and Chemistry of Minerals **30**, 463-468 (2003).

[29] Mansfield, R., and Williams, W. *The electrical properties of Bismuth Telluride.* Proc. Phys. Soc., **72**, 733-741 (1958).

[30] Mao, H.K., Xu, J., and Bell, P.M. *Calibration of the Ruby Pressure Gauge to 800 kbar under Quasi-Hydrostatic Conditions.* Journal of Geophysical Research, **91**, 4673-4676 (1986).

[31] Marchenkov, E.A., and Shipul', V.P. *Thermal Expansion of Semiconductor Materials.* Journal of Engineering Physics and Thermophysics, **66**, 547-551 (1994).

[32] Materials Data, Inc. *Jade: XRD Pattern Processing, Identification, and Quantification,* copyright, 1995-2006.

[33] Mishra, S.K., Satpathy, S., and Jepsen, O. *Electronic structure and thermoelectric properties of bismuth telluride and bismuth selenide.* Journal of Physics: Condensed Matter, **9**, 461-470 (1997).

[34] Nolas, G.S., Sharp, J., and Goldsmid, H.J. *Thermoelectrics: Basic Principles and New Materials Developments.* Springer-Verlag, 2001.

[35] Novikov, D.L., Katsnelson, M.I., Yu, J., Postnikov, A.V., and Freeman, A.J. *Pressure-induced phonon softening and electronic topological transition in* $HgBa_2CuO_4$. Physical Review B, **54**, 1313-1319 (1996).

[36] Osako, M. and Ito, E. *Simultaneous thermal diffusivity and thermal conductivity measurements of mantle materials up to 10 GPa.* Technical Report of ISEI, **67**, 1997.

[37] Pawlewicz, W.T., Rayne, J.A., and Ure, R.W. Jr. *Resistivity of* Bi_2Te_3 *from 1.3 K to 300 K* Physics Letters, **48A**, 391-392 (1974).

[38] Piermarini, G.J., Block, S., Barnett, J.D., and Forman, R.A. *Calibration of the pressure dependence of the R1 ruby fluorescence line to 195 kbar.* Journal of Applied Physics, **46**, 2774-2780 (1975).

[39] Polvani, D.A., Meng, J.F., ChandraShekar, N.V., Sharp, J., and Badding, J.V. *Large Improvement in Thermoelectric Properties in Pressure-Tuned p-type* $Sb_{1.5}Bi_{0.5}Te_3$. Chemistry of Materials, **13**, 2068-2071 (2001).

[40] Ragan, D.D., Clarke, D.R., and Schiferl, D. *Silicone fluid as a high-pressure medium in diamond anvil cells.* Review of Scientific Instruments, **67**, 494-496 (1996).

[41] Richter, W., Kohler, H., and Becker, C.R. *A Raman and Far-Ifrared Investigation of Phonons in the Rhombohedral* V_2-VI_3 *Compounds.* Physica Status Solidi B, **84**, 619-628 (1977).

[42] Rowe, D.M. *CRC Handbook of Thermoelectric Materials.* CRC Press, 1995.

[43] Scheidemantel, T.J., Meng, J.F., and Badding, J.V. *Thermoelectric power and phase transition of polycrystalline* As_2Te_3 *under pressure.* Journal of Physics and Chemistry of Solids, **66**, 1744-1747 (2005).

[44] Shen, Y.R. , Kumar, R.S., Pravica, M., and Nicol, M.F. *Characterisctics of silicone fluid as a pressure transmiting medium in diamond anvil cells.* Review of Scientific Instruments, **75**, 4450-4454 (2004).

[45] Venkatasubramanian, R., Silvola, E., Colpitts, T., and O'Quinn, B. *Thin-film thermoelectric devices with high room-temperature figures of merit.* Nature, **413**, 597-602, 2001.

[46] Vereshchagin, L.F., Atabaeva, E.Y., and Bendeliani, N.A. *Investigation of the Bi_2Te_3 phase diagram at high temperatures and pressures.* Soviet Physics-Solid State, **13**, 2051-2053 (1972).

[47] White, Mary Anne. *Properties of Materials.* Oxford University Press, 1999.

[48] Xie, H., Gu, H., Fujii, M., and Zhang, X. *Short hot wire technique for measureing thermal conductivity and thermal diffusivity of various materials.* Measurement Science and Technology, **17**, 208-214 (2006).

[49] Yamashita, Osamu, and Sugihara, Sunao. *High-performance bismuth-telluride compounds with highly stable thermoelectric figure of merit.* Journal of Materials Science, **40**, 6439-6444 (2005).

[50] Yousuf, M., and Rajan, K.G. *Principle of Massive Support in the opposed anvil high pressure apparatus* Pramana **18**, 1-15 (1982).

VITA

Graduate College
University of Nevada, Las Vegas

Matthew K. Jacobsen

Local Address:
8985 S. Durango Dr. Unit 1013
Las Vegas, Nevada 89113

Bachelors of Science, Physics, 2004
Oregon State University
Corvallis, Oregon

Publications:

Hamlin, J.J., Deemyad, S., Schilling, J.S., Jacobsen, M.K., Kumar, R.S., Cornelius, A.L., Cao, G., and Neumeier, J.J. *Studies on the weak itinerant ferromagnet* $SrRuO_3$. Physical Review B, Submitted 9/6/06

Thesis Title: Transport and Structural Studies of the thermoelectric material, Bi_2Te_3

Thesis Committee:
Committee Chairperson: Dr. Andrew Cornelius, Ph.D.
Committee Member: Dr. Lon Spight, Ph.D.
Committee Member: Dr. Michael Pravica, Ph.D.
Graduate Faculty Representative: Dr. Allen Johnson, Ph.D.